*Journal of Ceramic Processing Research. Vol. 15, No. 3, pp. 162~166 (2014)*

JOURNAL OF
**Ceramic Processing Research**

# Luminescence characteristics of red $Mg_{6-x}BP_5O_{20} : xEu^{3+}$ phosphors synthesized by solution combustion method

**H. Kim and K. Park***

*Faculty of Nanotechnology and Advanced Materials Engineering, Sejong University, Seoul 143-747, Korea*

**$Eu^{3+}$-doped $Mg_6BP_5O_{20}$ phosphors are prepared by solution combustion method. In this study, we investigate the microstructure and photoluminescence properties of $Mg_{6-x}BP_5O_{20} : xEu^{3+}$ ($0.025 \le x \le 0.1$) phosphors, depending on $Eu^{3+}$ content. The $Mg_{6-x}BP_5O_{20} : xEu^{3+}$ phosphors show high-quality powder characteristics, i.e., small size, spherical morphology, and narrow particle size distribution. The $Mg_{6-x}BP_5O_{20} : xEu^{3+}$ is effectively excited by near-UV (about 397 nm) and then emits red light. $Mg_{5.925}BP_5O_{20} : 0.075Eu^{3+}$ phosphor shows the strongest emission intensity among prepared phosphors. The $Mg_{6-x}BP_5O_{20} : xEu^{3+}$ is strongly desirable as a red phosphor for white light-emitting diodes.**

**Key words: Phosphor LEDs, $Eu^{3+}$-doped phosphor, 4f-4f transition, Phosphates.**

## Introduction

In recent years, significant attention has been paid to the development of white light-emitting diodes (LEDs) due to a long lifetime, high rendering index, high luminous efficiency, low power consumption, and concurrent reduction in environment pollution, allowing their wide application in consumer electronics and solid state lighting [1-3]. At present, a white-light LED with a blue InGaN chip in combination with a yellow phosphor ($Y_3Al_5O_{12} : Ce^{3+}$) is commercially available [1]. However, such a combination exhibits a low luminous efficiency and a poor color rendering index (< 80) because of the lack of a red light component [4, 5]. In addition, a white LED can be realized by the combination of a near-UV or blue chip with blue, green, and red phosphors, called phosphor-converted LEDs (pc-LEDs), yielding a high color rendering index and color reproducibility [6, 7]. The pc-LEDs are promising due to low costs, simplicity of the control circuit, chromatic flexibility, high stability, and high efficiency [8, 9]. However, the efficiency of the currently applied sulfide-based red phosphors, such as $SrS:Eu^{3+}$ and $Y_2O_2S:Eu^{3+}$, under blue light excitation is low because the absorption maximum does not match with the pump LED wavelength. Therefore, it is necessary to obtain white emission by the appropriate combination of a near-UV LED and proper inorganic phosphors. The development of new efficient red phosphors with high absorption in the UV or blue wavelengths for white LEDs is of crucial importance.

Phosphate is a kind of stable crystalline compound which is suitable for forming polymer arranged in a series of rings or chains by P-O bonds, and is a strong candidate as a phosphor owing to its good photoluminescent characteristics and good thermal and chemical stability [10]. In particular, borophosphates, in which anions contain both boron-oxygen tetrahedron and phosphorus-oxygen tetrahedron with various combinations, have attracted considerable interest due to their potential applications as LED phosphors, mercury-free lamp phosphors, plasma display panel (PDP) phosphors, green phosphors in tricolor lamps, and scintillation materials [11]. Among the borophosphates, in this study $Mg_6BP_5O_{20}$ and $Eu^{3+}$ are selected as a host material and an activator ion for red emission, respectively. $Mg_{6-x}BP_5O_{20} : xEu^{3+}$ ($0.025 \le x \le 0.1$) phosphors are synthesized by the solution combustion method and their photoluminescent characteristics are studied, especially with a focus on the $Eu^{3+}$ content.

In general, the solid-state reaction method is suitable for large scale production. However, the resultant powders are usually characterized by inhomogeneity in composition, large size, and irregular morphologies. To solve these problems, they need high annealing temperatures, prolonged heating during annealing, or milling and sieving of synthesized powders. As a result, many attempts have been carried out to find alternative methods for the preparation of high-quality phosphors. Solution combustion synthesis is a promising method to prepare high-purity, small-sized, and spherical particle phosphors. In this work, we report on the photoluminescent behaviors of red-emitting $Mg_{6-x}BP_5O_{20} : xEu^{3+}$ ($0.025 \le x \le 0.1$) phosphors synthesized by the solution combustion method.

## Experimental

The solution combustion method was applied to

*Corresponding author:
Tel : +82-2-3408-3777
Fax: +82-2-3408-4342
E-mail: kspark@sejong.ac.kr

prepare red-emitting $Mg_{6-x}BP_5O_{20}$ : $xEu^{3+}$ ($0.025 \le x \le 0.1$) phosphors. $Mg(NO_3)_2 \cdot 6H_2O$ (99%, High Purity Chemicals), $H_3BO_3$ (99.9%, High Purity Chemicals), and $(NH_4)_2HPO_4$ (99.0%, Samchun Pure Chemical Co.) were used as the source of host materials. $Eu_2O_3$ (99.9%, High Purity Chemicals) was used as the activator. First, $Eu_2O_3$ was dissolved into concentrated $HNO_3$ (60%) to form $Eu^{3+}$ nitrate. Second, an appropriate amount of $Eu^{3+}$ nitrate, $Mg(NO_3)_2 \cdot 6H_2O$, $H_3BO_3$, $(NH_4)_2HPO_4$, and citric acid ($C_3H_4(OH)(COOH)_3$, Duksan Pure Chemical Co.) was dissolved in deionized water. Then, the obtained solutions were mixed and heated under magnetic stirring. After heating on a hot plate, foam appeared. Self-ignition and black smoke were observed, synthesizing $Mg_{6-x}BP_5O_{20}$ : $xEu^{3+}$ ($0.025 \le x \le 0.1$) powders. The synthesized powders were calcined at 300 °C to remove residual impurities. Subsequently, the powders were annealed at 1000 °C. The Fourier transform infrared (FT-IR) was performed with Thermo-Nicolet equipment in the 4000-650 $cm^{-1}$ region. The crystal structure of the syn-thesized and annealed $Mg_{6-x}BP_5O_{20}$ : $xEu^{3+}$ phosphors was analyzed with an X-ray diffractometer (XRD; Rigaku RINT 2000) with Cu Kα radiation ($\lambda = 0.15418$ nm). The morphological char-acteristics of the phosphors were investigated with a field emission scanning electron microscope (FE-SEM; Hitachi S4700). The pho-toluminescent spectra of the phosphors were obtained with a Spectrofluorometer (QM-4/2005SE, PTI, USA) equipped with a 75W Xenon lamp.

## Results and Discussion

A series of $Mg_{6-x}BP_5O_{20}$:$xEu^{3+}$ ($0.025 \le x \le 0.1$) phosphor powders is synthesized via the solution combustion method, using its corresponding metal nitrates as the oxidizers and citric acid as the combustion fuel as follows:

$$(6-x)Mg(NO_3)_2\ 6H_2O + xEu(NO_3)_3 + 5(NH_4)_2HPO_4 + H_3BO_3 + \frac{10}{3}C_3H_4(OH)(COOH)_3 \rightarrow Mg_{6-x}Eu_xBP_5O_{20} + 20CO_2 + 10NH_3 + 6N_2 + 55H_2O + \frac{5}{3}O_2 \quad (1)$$

The combustion method is favorable for producing nanocrystalline powders in a short time and at a low calcination temperature with improved powder char-acteristics.

The FT-IR spectra of synthesized and annealed $Mg_6BP_5O_{20}$ : $Eu^{3+}$ powders from 650 to 4000 $cm^{-1}$ are shown in Figs. 1(a) and (b), respectively. The absorption bands at 932 $cm^{-1}$ are assigned to the symmetric stretching mode of the P-O bond in $PO_4^{3-}$ group, and the bands at 1040 and 1084 $cm^{-1}$ correspond to the asymmetric stretching mode of the P-O bond in $PO_4^{3-}$ group [12]. The bands at 1300-1800 $cm^{-1}$ are attributed to the $CO_3^{2-}$ anion group, which comes from the citric acid used as a fuel [13]. Moreover, the bands at 2851 and 2931 $cm^{-1}$ are mainly due to the stretching of the C-H bonds [12]. It is found that the intensity of bands at 932, 1040, and 1084 $cm^{-1}$ for the annealed $Mg_6BP_5O_{20}$ : $Eu^{3+}$ powders is stronger than that for the synthesized $Mg_6BP_5O_{20}$ : $Eu^{3+}$ powders, whereas the intensity of bands at 1300-1800 $cm^{-1}$ for the annealed $Mg_6BP_5O_{20}$ : $Eu^{3+}$ powders is weaker than that for the synthesized $Mg_6BP_5O_{20}$:$Eu^{3+}$ powders.

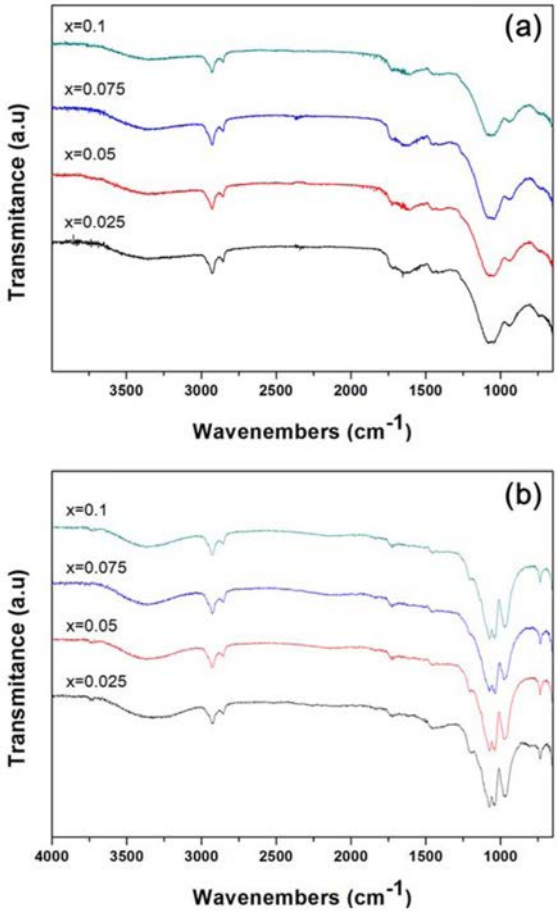


**Fig. 1.** FT-IR spectra of (a) synthesized and (b) annealed $Mg_{6-x}BP_5O_{20}$ : $xEu^{3+}$ ($0.025 \le x \le 0.1$) powders.

Fig. 2 shows the XRD patterns of the annealed $Mg_{6-x}BP_5O_{20}$ : $xEu^{3+}$ ($0.025 \le x \le 0.1$) phosphors. The $Mg_{6-x}BP_5O_{20}$ : $xEu^{3+}$ phosphors show quite similar XRD patterns, irrespective of $Eu^{3+}$ content. These results suggest that the addition of $Eu^{3+}$ has no significant influence on the crystal structure. In the literature, there exists no JCPDS card of $Mg_6BP_5O_{20}$ for comparison. Since the XRD patterns do not show the existence of the constituent nitrates and impurities, it seems that the annealed $Mg_{6-x}BP_5O_{20}$ : $xEu^{3+}$ forms the desired single phase. The crystallite size of the $Mg_{6-x}BP_5O_{20}$ : $xEu^{3+}$ powders can be calculated from the broadening of diffraction peaks by the following Scherrer's formula [14]:

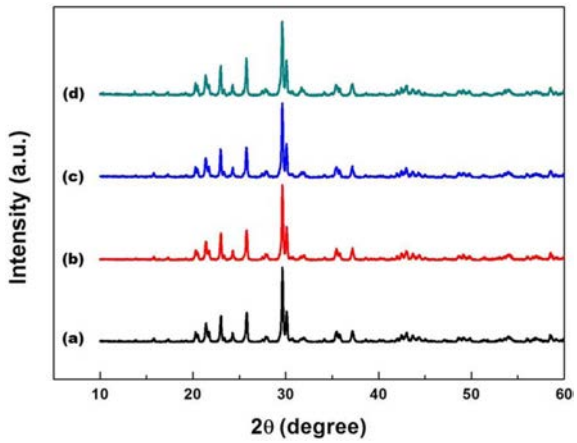


**Fig. 2.** XRD patterns of the annealed $Mg_{6-x}BP_5O_{20}:xEu^{3+}$ ($0.025 \le x \le 0.1$) phosphors: $x$ = (a) 0.025, (b) 0.05, (c) 0.075, and (d) 0.1.

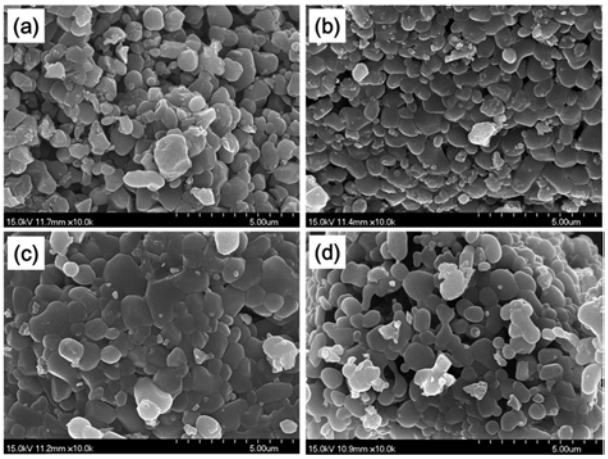


**Fig. 3.** FE-SEM images of the annealed $Mg_{6-x}BP_5O_{20}:xEu^{3+}$ ($0.025 \le x \le 0.1$) phosphors: $x$ = (a) 0.025, (b) 0.05, (c) 0.075, and (d) 0.1.

$$D=(0.9\lambda)/(\beta\cos\theta) \quad (2)$$

where λ is the wavelength of radiation, θ is the angle of the diffraction peak, and β is the full width at half maximum of the diffraction peak (in radian). The calculated crystallite sizes of the $Mg_{6-x}BP_5O_{20}:xEu^{3+}$ powders are fairly similar, i.e., 39.3, 39.7, 38.2, and 38.3 nm for $x = 0.025$, 0.05, 0.075, and 0.1, respectively.

FE-SEM images of the annealed $Mg_{6-x}BP_5O_{20}:xEu^{3+}$ ($0.025 \le x \le 0.1$) phosphors are shown in Fig. 3. The $Mg_{6-x}BP_5O_{20}:xEu^{3+}$ powders with different $Eu^{3+}$ contents possess very similar characteristics, i.e., small size, spherical morphology, and narrow particle size distribution. These powder characteristics are favorable for obtaining high brightness and high resolution due to the high packing densities and low scattering of light [14]. The combustion processing used here for synthesizing $Mg_{6-x}BP_5O_{20}:xEu^{3+}$ powders is fairly simple, fast, and cost-effective compared to conventional solid-state reaction method.

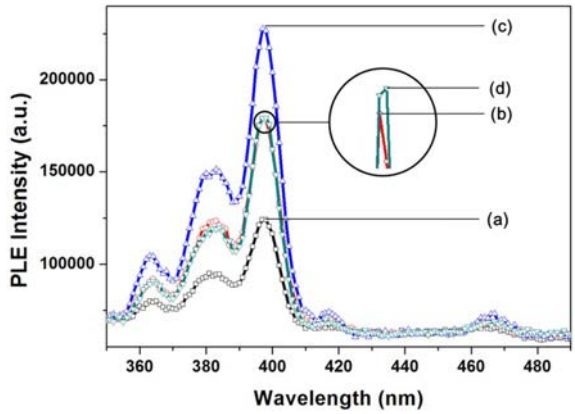


**Fig. 4.** Excitation spectra of the $Mg_{6-x}BP_5O_{20}:xEu^{3+}$ ($0.025 \le x \le 0.1$) phosphors, monitored at 592 nm: $x$ = (a) 0.025, (b) 0.05, (c) 0.075, and (d) 0.1.

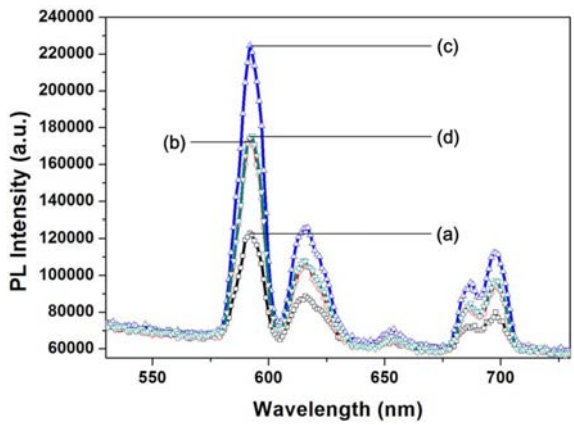


**Fig. 5.** Emission spectra of the $Mg_{6-x}BP_5O_{20}:xEu^{3+}$ ($0.025 \le x \le 0.1$) phosphors, recorded under the 397 nm: $x$ = (a) 0.025, (b) 0.05, (c) 0.075, and (d) 0.1.

The excitation spectra of the $Mg_{6-x}BP_5O_{20}:xEu^{3+}$ ($0.025 \le x \le 0.1$) phosphors, monitored at 592 nm, are shown in Fig. 4. Several strong sharp peaks are found in the 350-500 nm which are attributed to the intra-configurational 4f-4f transitions of $Eu^{3+}$ ions in the host lattices. The excitation peaks centered at 363, 383, 397, 417, and 466 nm are caused by the $^7F_0 \rightarrow {}^5D_4$, $^7F_0 \rightarrow {}^5L_7$, $^7F_0 \rightarrow {}^5L_6$, $^7F_0 \rightarrow {}^5D_3$, and $^7F_0 \rightarrow {}^5D_2$ transitions, respectively [10, 15]. Among them, the intensity of the peak at 397 nm is much stronger than that of the others. This indicates that near-UV light (397 nm) can be strongly absorbed, which is in good agreement with the near-UV LED chips.

The emission spectra of the $Mg_{6-x}BP_5O_{20}:xEu^{3+}$ ($0.025 \le x \le 0.1$) phosphors, recorded under the 397 nm excitation, are shown in Fig. 5. For the $Mg_{6-x}BP_5O_{20}:xEu^{3+}$ phosphors with different $Eu^{3+}$ contents, the shapes of the emission peaks are quite similar, whereas their intensities are different. The emission peaks are located at 592, 617, 654, and 698 nm. The four peaks correspond to the transitions from the excited $^5D_0$ to $^7F_J$ (J = 1, 2, 3, and 4) levels in $4f^6$ configuration of $Eu^{3+}$ [15]. The emission intensity caused by the

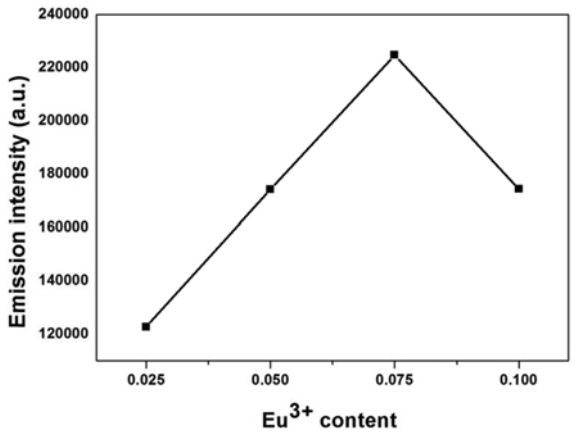


**Fig. 6.** Emission intensities, centered at 592 nm, of the $Mg_{6-x}BP_5O_{20}$ : $xEu^{3+}$ ($0.025 \le x \le 0.1$) phosphors.

$^5D_0 \rightarrow {}^7F_1$ transition is stronger than that caused by the $^5D_0 \rightarrow {}^7F_2$ transition. This means that $Eu^{3+}$ is located in the high symmetry site with inversion center of the host lattice [16]. The intensity ratio of $^5D_0 \rightarrow {}^7F_2$ to $^5D_0 \rightarrow {}^7F_1$, i.e. the asymmetry ratio, represents how far the $Eu^{3+}$ local surroundings deviate from centrosymmetry [17].

In the $Mg_{6-x}BP_5O_{20}$ : $xEu^{3+}$ phosphors, one $Eu^{3+}$ ion is supposed to replace one $Mg^{2+}$ ion. It is important to note that the replacement of divalent $Mg^{2+}$ by trivalent $Eu^{3+}$ in the $Mg_{6-x}BP_5O_{20}$ : $xEu^{3+}$ phosphors induces charge unbalance. It is thus difficult to keep charge balance in the phosphors [18-20]. Herein, we propose two charge compensation models: (1) Three $Mg^{2+}$ ions are replaced by two $Eu^{3+}$ ions, with charge compensation provided by an Mg vacancy ($3Mg^{2+} \rightarrow 2Eu^{3+}$ + vacancy). This charge compensation yields additional vacancy sites. Therefore, the energy absorbed from the charge-transfer state is inefficiently transferred to $Eu^{3+}$ ions by the non-radiative sites [18]. (2) Two $Mg^{2+}$ ions are replaced by one $Eu^{3+}$ and one monovalent ion ($M^+$) such as $Li^+$, $Na^+$, and $K^+$ ($2Mg^{2+} \rightarrow Eu^{3+} + M^+$). Here, $M^+$ acts as a charge compensator. We can expect that the emission intensity of the $^5D_0 \rightarrow {}^7F_2$ transition is able to be significantly increased by the efficient charge compensation.

The emission intensities, centered at 592 nm, of the $Mg_{6-x}BP_5O_{20}$ : $xEu^{3+}$ ($0.025 \le x \le 0.1$) phosphors as a function of $Eu^{3+}$ content are shown in Fig. 6. It can be clearly seen that the emission intensity depends strongly on the content of $Eu^{3+}$ ions. The emission intensity increases with $Eu^{3+}$ content up to $x = 0.075$ due to the larger number of luminescent centers and then decreases with the further increased $Eu^{3+}$ content, owing to the energy transfer between the neighboring $Eu^{3+}$ ions, i.e., quenching of the emission of $Eu^{3+}$ [21]. The emission intensity of $Mg_{5.925}BP_5O_{20}$ : $0.075Eu^{3+}$ phosphors, centering at 592 nm, is approximately two times stronger than that of $Mg_{5.975}BP_5O_{20}$ : $0.025Eu^{3+}$ phosphors. These results suggest that the emission properties of the $Mg_{6-x}BP_5O_{20}$ : $xEu^{3+}$ phosphors are enhanced by controlling the $Eu^{3+}$ content. The $Mg_{6-x}BP_5O_{20}$ : $xEu^{3+}$ is suitable for use as a red phosphor for white LEDs.

## Conclusions

The $Mg_{6-x}BP_5O_{20}$:$xEu^{3+}$ ($0.025 \le x \le 0.1$) phosphors showed small size, spherical morphology, and narrow particle size distribution. The excitation spectra of the $Mg_{6-x}BP_5O_{20}$ : $xEu^{3+}$ phosphors, monitored at 543 nm, showed several strong peaks at 363 nm ($^7F_0 \rightarrow {}^5D_4$), 383 nm ($^7F_0 \rightarrow {}^5L_7$), 397 nm ($^7F_0 \rightarrow {}^5L_6$), 417 nm ($^7F_0 \rightarrow {}^5D_3$), and 466 nm ($^7F_0 \rightarrow {}^5D_2$). The intensity of the peak at 397 nm was the strongest among them. This indicates that the $Mg_{6-x}BP_5O_{20}$ : $xEu^{3+}$ phosphors can be efficiently excited by near-UV InGaN chips. Upon excitation with 397 nm (near-UV light), the emission peaks were located at about 592 nm ($^5D_0 \rightarrow {}^7F_1$), 617 nm ($^5D_0 \rightarrow {}^7F_2$), 654 nm ($^5D_0 \rightarrow {}^7F_3$), and 698 nm ($^5D_0 \rightarrow {}^7F_4$). The emission intensity increased with an increase in $Eu^{3+}$ content up to $x = 0.075$ and then decreased with further increase of $Eu^{3+}$ content. The $Mg_{6-x}BP_5O_{20}$ : $xEu^{3+}$ had a high potential as a red phosphor for white LEDs.

## References

1. S. Yan, J. Zhang, X. Zhang, S. Lu, X. Ren, Z. Nie, and X. Wang, J. Phys. Chem. C 111 (2007) 13256-13260.
2. X. Zhang, X. Wang, J. Huang, J. Shi, and M. Gong, Opt. Mater. 32 (2009) 75-78.
3. R. Hu, X. Luo, H. Feng, and S. Liu J. Lumin. 132 (2012) 1252-1256.
4. Z.L. Wang, H.B. Liang, L.Y. Zhou, J. Wang, M.L. Gong, and Q. Su, J. Lumin. 128 (2008) 147-154.
5. F.A. Ponce and D.P. Bour, Nature 386 (1997) 351.
6. J.K. Park, M.A. Lim, C.H. Kim, H.D. Park, J.T. Park, and S.Y. Choi, Appl. Phys. Lett. 82 (2003) 683.
7. Y.D. Huh, J.H. Shim, Y. Kim, and Y.R. Do, J. Electrochem. Soc. 150 (2003) H57-H60.
8. J.S. Kim, P.E. Jeon, Y.H. Park, J.C. Choi, H.L. Park, G.C. Kim, and T.W. Kim, Appl. Phys. Lett. 85 (2004) 3696.
9. M. Bredol, U. Kynast, and C. Ronda, Adv. Mater. 3 (1991) 361-367.
10. R. Wang, L. Zhou, and Y. Wang, J. Rare Earths 29 (2011) 1045-1048.
11. C. Qin, Y. Huang, W. Zhao, L. Shi, and H. J. Seo, Mater. Chem. Phys. 121 (2010) 286-290
12. O. Kaygili, C. Tatar, and F. Yakuphanoglu, Ceramics International 38 (2012) 5713-5722.
13. N. Dhananjaya , H. Nagabhushana, B.M. Nagabhushana, B. Rudraswamy, S.C. Sharma, D.V. Sunitha, C. Shivakumara, and R.P.S. Chakradhar, Spectrochimica Acta Part A: Molecular and Biomolecular Spectroscopy 96 (2012) 532540.
14. Y.H. Zhou and J. Lin, Opt. Mater. 27 (2005) 1426-1432.
15. B.S. Tsai, Y.H. Chang, and Y.C. Chen, J. Alloys and Compounds 407 (2006) 289-293.
16. Z. Wei, L. Sun, C. Liao, J. Yin, X. Jiang, C. Yan, and S. Lu, J. Phys. Chem. B 106 (2002) 10610-10617.
17. J. Chen, J. Wang, F. Zhang, D. Yan, G. Zhang, R. Zhuo,

and P. Yan, J. Phys. D: Appl. Phys. 41 (2008) 105306.
18. S. Choi, Y.-M. Moon, H.-K. Jung, Mater. Res. Bull. 45 (2010) 118-120.
19. S. Shi, J. Gao, J. Zhou, Opt. Mater. 30 (2008) 1616-1620.
20. Z. Mu, Yihua Hu, L. Chen, X. Wang, Opt. Mater. 34 (2011) 89-94.
21. M. Weng, R. Yang, Y. Peng, and J. Chen, Ceramics International 38 (2012) 1319-1323.